GEOPHYSICS, VOL. 74, NO. 5 (SEPTEMBER-OCTOBER 2009); P. F77–F87, 10 FIGS., 2 TABLES.
10.1190/1.3173807

Casing effects in the sea-to-borehole electromagnetic method

F. N. Kong[1], F. Roth[2], P. A. Olsen[3], and S. O. Stalheim[3]

ABSTRACT

The sea-to-borehole controlled source electromagnetic (CSEM) method has the potential of becoming a useful new exploration and monitoring technique. Modeling shows that the electromagnetic fields at reservoir depths can be 1-2 orders of magnitude larger than those on the seabed, thus opening up the possibility to see deeper or detect and monitor smaller targets. In the case of measurements inside metal casing, the use of reciprocity to interchange the source and receiver allows the casing conductor to be considered as an antenna. This antenna is excited by a source inside the casing, which induces a current flowing along the casing conductor. Based on the current distribution, a casing dipole moment and an equivalent length were derived for the transverse magnetic (TM) mode. In the frequency range of interest (0.1–10 Hz), the increase in field strength (resulting from sea-to-borehole measurements) is not lost to the casing attenuation for either the TM or the transverse electric (TE) mode. The ratio of the dipole moment of the casing antenna to that of the source current can be considered as the casing attenuation effect. This ratio is not far from unity for frequencies smaller than 1 Hz, but it decreases rapidly with frequency. The equivalent length of the casing antenna can be of the order of a few hundred meters. As a consequence, the field distribution changes significantly in the presence of casing, and the vertical resolution of TM measurements is degraded. The horizontal resolution is not degraded significantly. Measurement of the TM mode has the advantage of being sensitive to thin resistive targets and being less affected by sea-air interactions in shallow water. The TE mode measurement, having a localized casing effect, contributes valuable information about the background resistivity.

INTRODUCTION

During recent years, the marine controlled-source electromagnetic (CSEM) method has emerged as a useful method to locate high resistive targets, such as hydrocarbon layers (Eidesmo et al., 2002; Ellingsrud et al., 2002; Kong et al., 2002; Constable and Srnka, 2007) and subbasalt structures (MacGregor and Sinha, 2000). In a typical marine CSEM measurement, a vessel tows the source antenna and the receiver sensors are placed on the seabed. Lately, marine CSEM has been suggested for monitoring purposes (Lien and Mannseth, 2008; Orange et al., 2009) and field appraisal (Stalheim and Olsen, 2008). These new applications might benefit from placing the receivers (or the source) in a borehole, where they are closer to the target to be characterized (Figure 1). Such measurement could be referred to as the sea-to-borehole electromagnetic (EM) method, which is the topic here. Recent publications on similar topics can be found (Scholl and Edwards, 2007; Pardo et al., 2008; Stalheim and Olsen, 2008).

Methods using EM signals to perform crosswell and borehole-to-surface measurements were presented many years ago (Zhou, 1989; Alumbaugh and Morrison, 1995; Newman, 1995; Spies and Habashy, 1995; Wilt et al., 1995; Hoversten et al., 2001). In these applications, the frequency range typically is 100 Hz to 1000 Hz, and the detection distance is in the range of a few hundred meters. The most frequently reported source type used inside a borehole is a magnetic dipole, which generates a magnetic field along the borehole direction (transverse electric [TE] field). For the convenience of description, in this study these applications are referred to as high-frequency (HF) applications. Here, we discuss sea-to-borehole measurements using frequencies lower than these HF applications. A typical survey scenario for our application is given by the following set of parameters: frequency 0.1–10 Hz, source-receiver offset 0–10 km, target (high-resistive layers) depth 1–3 km, and receiver deployment inside a vertical steel-cased borehole.

In a cased borehole environment, the problem of measuring inside a steel casing must be considered. During the development of the HF

Manuscript received by the Editor 21 December 2008; revised manuscript received 22 March 2009; published online 21 August 2009.
[1]Norwegian Geotechnical Institute, Oslo, Norway. E-mail: fk@ngi.no.
[2]EMGS, Trondheim, Norway. E-mail: froth@emgs.com.
[3]StatoilHydro ASA, Trondheim, Norway. E-mail: PEAO@StatoilHydro.com; STOS@StatoilHydro.com.

crosswell measurement, the casing effect has been studied in detail and many results have been published (Augustin et al., 1989; Uchida et al., 1991; Wu and Habashy, 1994; Wilt et al., 1995; Becker et al., 1997; Lee et al., 2005; Pardo et al., 2007; Pardo et al., 2008).

The casing problem has been investigated in another application, i.e., the resistivity measurement through casing (Kaufman, 1990; Kaufman and Wightman, 1993; Schenkel and Morrison, 1994; Singer and Strack, 1998; Pardo et al., 2007; Pardo et al., 2008). Very low frequency or DC is used in this application, which is referred to as the DC application in subsequent discussions.

It is interesting to note that only the transverse magnetic (TM) mode is considered in the DC application, whereas in HF applications, the TE mode is discussed most frequently (Augustin et al., 1989; Uchida et al., 1991; Wilt et al., 1995; Becker et al., 1997). The likely reason for this is that the sources used for HF applications typically are magnetic dipoles oriented along the borehole direction. The casing effects for the TM mode for the non-DC case have received less attention in the literature. In our application, the TM mode is very important because a thin hydrocarbon layer can support only the TM mode (Løseth and Amundsen, 2007; Kong et al., 2007, 2008). Analyzing the casing effects for the TM mode is therefore the main topic here. Arbitrarily shaped geologic targets, however, might support both TM and TE modes.

In the theory of resistivity measurement through casing (Kaufmann, 1990), the frequency is assumed to be zero. This imposes a limitation to the method. For instance, in the DC approximation, a major disadvantage is that the fields calculated are not a function of the magnetic casing properties. In our method, we keep the frequency as a variable, and the DC solution is used only to compare with our solution at the low-frequency end.

We adopt a new approach to investigate the casing effect. We use reciprocity to interchange the source and receiver, allowing us to consider the casing conductor as an antenna. This antenna is excited by a source inside the casing, which induces a current flowing on the casing conductor. Based on the current distribution, a "casing" dipole moment and an equivalent length are derived for the TM mode, which are used to evaluate the casing effects.

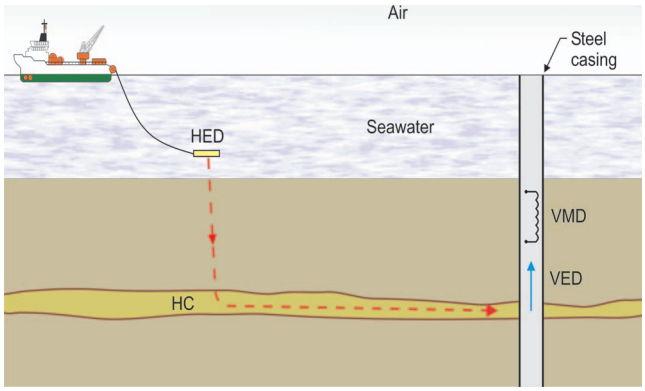

Figure 1. Test layout of sea-to-borehole measurement, whereby a horizontal electric dipole (HED) is pulled by a vessel in the sea and excites electromagnetic fields. The fields reflected and refracted by a hydrocarbon layer (HC) are received by a vertical electric dipole (VED) and a vertical magnetic dipole (VMD) placed inside a steel-cased borehole.

SEA-TO-BOREHOLE MEASUREMENT FOR CHARACTERIZING A RESISTIVE LAYER

Consider two measurement cases, both with a horizontal electric dipole (HED) source towed by a vessel in the sea, as illustrated in Figure 1. In case 1, the receiver is placed in a vertical borehole: the sea-to-borehole case. In case 2, the receiver is placed on the seabed: the sea-to-seabed case.

The receiver will sense the target responses while the source changes location. A monitoring task can be, for example, to find the changes of the target properties (length, resistivity, and so on) by comparing the target responses measured at different times, while keeping the source towline unchanged. Other applications can be appraisal of discoveries and identification of remaining small reservoirs (Stalheim and Olsen, 2008).

The coordinate system used in the following is z as the vertical axis, with $z = 0$ at seabed, x as the in-plane horizontal axis, and y as the horizontal axis normal to x.

We consider first the 1D target problem — a highly resistive layer of infinite extent. The analytic solution for a dipole antenna embedded inside a 1D anisotropic layered medium is known (Wait, 1966; Kong, 1972, 1990) and can be used to calculate the fields in each layer. The implementation of the method can be found in Kong et al. (2008).

The results shown in Figure 2 are obtained by the above-mentioned analytic method. Shown are the received E_z and H_y fields for the sea-to-borehole case and the E_x and H_y fields for the sea-to-seabed case for the following model: target depth 1300 m, target thickness 100 m, target resistivity 50 ohm-m, frequency 1 Hz, seabed resistivity 1 ohm-m, seawater resistivity 0.3 ohm-m, and water depth 10 km. The source HED is 50 m above the seabed. The receiver is inside the target layer for the sea-to-borehole case and on the seabed for the sea-to-seabed case. We intentionally have set the seawater to be very deep for the purpose of comparing against the shallow-water case. In the figure, the "offset" is defined as the horizontal distance between the source and the receiver.

The reason for choosing these field components for comparison is that only TM fields (E_x, E_z, H_y) are excited inside a thin, horizontal, and highly resistive layer (Løseth and Amundsen, 2007; Kong et al., 2007, 2008). Hence for detecting such layers, the TM fields are more important than the TE fields, no matter whether the sea-to-borehole measurement or the sea-to-seabed measurement is used. In real cases, however, the target might be an arbitrary 3D body. It might support both TM and TE modes.

It is known also that for the sea-to-seabed case, using the inline E field (i.e., E_x) is more effective than using the E_z field in detecting the target response (Chave and Cox, 1982). However, because a pair of electrodes normally is used to detect the E field and the received voltage is proportional to the spacing between the two electrodes, E_z should be measured inside a vertical well for the sea-to-borehole case. The E_x field likewise could be measured in a horizontal well. It is possible to achieve a long spacing only when the electrodes are placed along the borehole direction. That is why in Figure 2 we compare the inline field E_x of the sea-to-seabed case with the vertical field E_z of the sea-to-borehole case.

From Figure 2a, it can be seen that the E_z field inside a borehole at the target location is about 100 times larger than the inline E field received at the seabed for large offsets. In addition, the H_y field inside a borehole at the target location is about 10 times larger than the H_y field on the seabed. This demonstrates one of the advantages of using

sea-to-borehole measurement: the received signal is larger than in the sea-to-seabed case on far offsets.

For an HED source, the vertical electric field (E_z) is not sensitive to the refracted airwave. Hence, the E_z signal received in the sea-to-borehole case is less influenced by the air-sea interface than the E_x signal in the sea-to-seabed case. This can be observed in Figure 2b, showing results for the same modeling parameters as in Figure 2a except that the water depth is 500 m. Note that E_x for the shallow-water case is very different from the deepwater case, whereas E_z at the target depth has not changed significantly. This is another advantage of sea-to-borehole measurements compared to sea-to-seabed measurements.

Figure 3 shows the received E_z signal at target depth as a function of the offset between the source and the receiver for various target resistivities. The curves are different, which forms the basis for using sea-to-borehole measurements to monitor the resistivity change of the target layer.

The analytic method mentioned above can be used only for solving the 1D target problem. For more complicated 2D and 3D cases, numerical methods must be used. Figure 4 shows the E_z, E_x, and H_y field magnitude distributions generated by an HED above the seabed for a 2D reservoir at $z = 1000$ m below seabed (conductivities and thickness as given above) and extending from $x = 250$ m to $x = 2750$ m. In this case, the water depth is 500 m and the HED is 50 m above the seabed. Because the target is two-dimensional, it is a 2.5D problem, which is modeled using the method described in Kong et al. (2008). The target location is clearly visible in the E_z distribution. The color scale is in an index-10 logarithmic scale. From Figure 4, it can be seen that for measuring the target response, one should measure one or more of the following: E_z inside the target or nearby the target; E_x nearby, but outside the target or at the seabed; H_y inside the target, nearby the target or at the seabed.

The above discussion is based on the assumptions that the target is aligned along the x-direction, no variation occurs along the y-direction, and the borehole is oriented along the z-direction. In practice, many of the above assumptions might not be satisfied. Hence, both TM and TE fields should be measured.

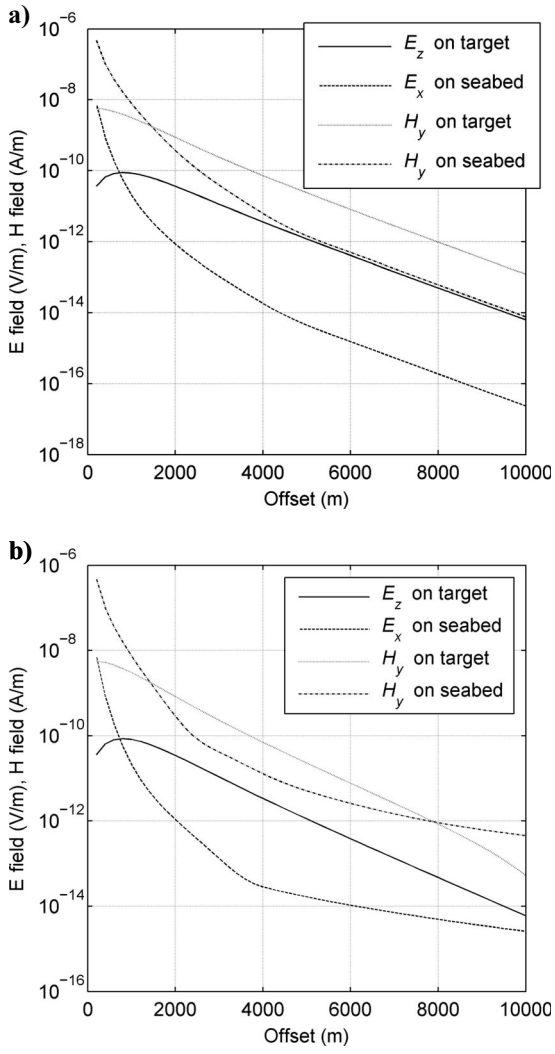

Figure 2. EM field magnitudes versus offset at reservoir depth (on target) and on seabed for water depths (a) 10 km and (b) 0.5 km. The other model parameters are: source (1 Hz-HED and 50 m above seabed), target (top reservoir depth 1300 m, thickness 100 m, resistivity 50 ohm-m), seabed (resistivity 1 ohm-m), and seawater (resistivity 0.3 ohm-m).

THE CASING EFFECT: TM MODE

Modeling method

The analytic method for calculating the fields inside a cylindrically layered medium with a source at the center of the medium is well known (Chew, 1995). For the TM mode, the method is discussed in detail by Wait (1982), Kaufman (1990), and Kaufman and Wightman (1993). In their discussions, however, only the DC case is considered. The method for the TE mode considering the frequency effect is discussed in detail by Augustin et al. (1989), Uchida et al. (1991), Becker et al. (1997), and Lee et al. (2005). In Appendix A, we use the analytic method to solve for the TM fields for the non-DC case.

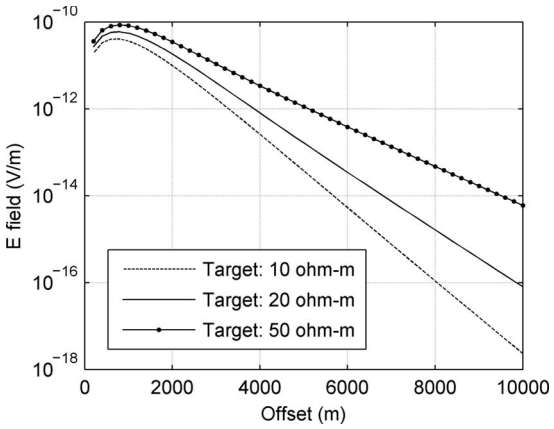

Figure 3. Vertical electric field (E_z) magnitude versus offset at reservoir depth (target) for three target resistivities. The test layout is the same as for Figure 2 (shallow-water case).

Consider an electric current source along the z-direction inside an infinitely long and cylindrical steel casing with the following model parameters:

σ_1: conductivity of the borehole fluid
σ_2: conductivity of the steel casing
σ_3: conductivity of the formation
$\mu = \mu_r \mu_0$: magnetic permeability of the casing
$\mu_0 = 4\pi 10^{-7}$ H/m: magnetic permeability inside and outside the casing.

Following the procedure outlined in Appendix A, the fields of the TM mode outside the casing can be obtained as

$$\hat{H}_\phi = a_3 \sigma_3 k_3 K_1(k_3 \rho), \tag{1}$$

$$\hat{E}_\rho = a_3 \lambda k_3 K_1(k_3 \rho), \tag{2}$$

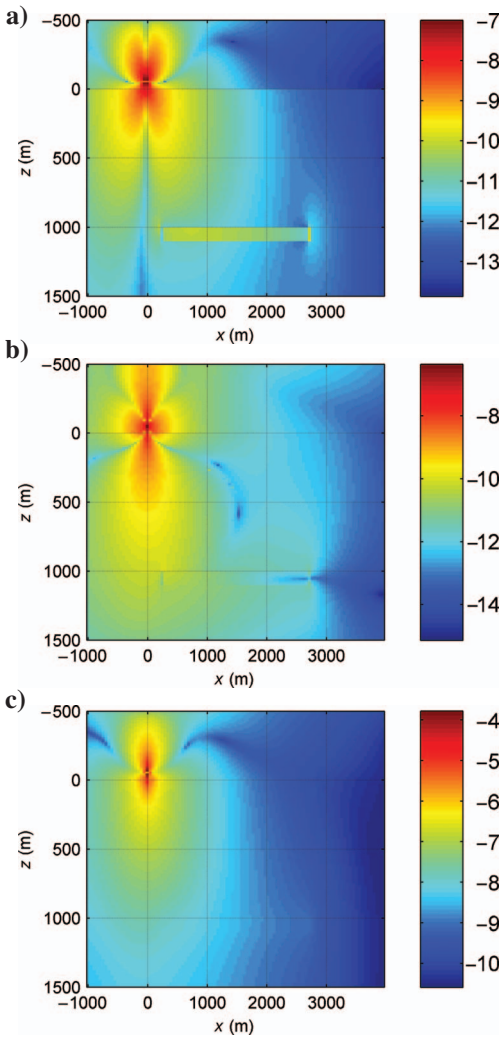

Figure 4. The EM field distributions, generated by a 1 Hz HED located 50 m above the seafloor. (a) vertical electric field (E_z) (color scale $\log_{10}(|E_z|)$), (b) horizontal electric field (E_x) (color scale $\log_{10}(|E_x|)$), and (c) horizontal magnetic field (H_y) (color scale $\log_{10}(|H_y|)$). The 2D target is located at $z = 1000$ m, $x = 250$–2750 m, and with the same thickness and resistivity as the target considered for Figure 2.

$$\hat{E}_z = -a_3 k_3^2 K_0(k_3 \rho). \tag{3}$$

Here ρ is radial distance from the center of the borehole; k_3 is the radial wavenumber in layer 3 defined in A-11 in Appendix A; K_1 and K_0 are the second modified Bessel functions of orders 1 and 0, respectively; and a_3 is the coefficient for outgoing waves in layer 3 determined by the boundary conditions.

The fields in equations 1–3 are in the wavenumber domain. The corresponding fields in the space domain can be obtained by using the Fourier cosine transform defined in equation A-5 for the even function fields such as $\hat{H}_\phi$ and $\hat{E}_z$, and using the Fourier sine transform for the odd function field $\hat{E}_\rho$.

We have made a simple check of the calculation by setting σ_1, σ_2, $\sigma_3 = 1$ S/m and comparing the H_ϕ field obtained by applying the Fourier cosine transform to equation 1 to the analytic result (Wait, 1987)

$$H_\phi = \frac{IL}{4\pi r^2}(1 + ikr)e^{-ikr} \sin\theta, \tag{4}$$

where $r = (\rho^2 + z^2)^{1/2}$, $\sin\theta = \rho/r$, and $k^2 = -i\omega\mu\sigma$.

The comparison shows that for $\rho = 0.15$ m and $z = 1$–1000 m, the relative error between the H_ϕ magnitudes of the numerical result and the analytic result is smaller than 10^{-5}. It should be noted that using the fast Fourier transform (FFT) algorithm for evaluating the Fourier cosine transform would require many $\bar{\lambda}$ samples to reach a small relative error for the weak-signal region at large offset. This results from the truncation and cyclic errors of the FFT. Because the transmission and reflection coefficients b_1, a_2, b_2, and a_3 must be calculated for each $\bar{\lambda}$ based on the boundary conditions (see Appendix A), many $\bar{\lambda}$ samples mean a large computational effort. Hence, it is advantageous to use the digital-filter technique (Kong, 2007) to evaluate the cosine integral. We have used a filter using 241 $\bar{\lambda}$ points and achieved an accurate evaluation of the Fourier cosine transform.

Modeling results: Field distributions

In the following, we use these standard model parameters unless specified otherwise: frequency (f) = 1 Hz, casing inner radius (s) = 0.1 m, casing outer radius (t) = 0.11 m, $\sigma_1 = 1$ S/m, $\sigma_2 = 5(10^6)$ S/m, $\sigma_3 = 1$ S/m, and the relative magnetic permeability of the casing (μ_r) = 100. The relative magnetic permeability of the borehole fluid and the formation is assumed to be unity.

Figure 5 shows the H_ϕ field magnitude distributions in the vertical plane for cases with and without a steel casing. The difference between the field distributions of these two cases can be seen clearly. Without casing, the behavior of H_ϕ is as in equation 4, and the field is very weak along the borehole direction. In contrast, with casing, the H_ϕ field along the borehole direction no longer is very weak. Figure 6 shows the E_z field distributions, and Figure 7 shows the E_ρ field distributions with and without casing.

The general feature one might observe from these figures is that the fields H_ϕ and E_ρ at small ρ and large z are much stronger with casing than without casing. This might be explained by the fact that a single metal cylinder can support a guided wave (Stratton, 1941). In other words, a current is flowing along the casing, which is induced by the current source placed inside the casing. According to Ampere's law, this results in a strong H_ϕ field. Figure 8 is used to show a more precise comparison for the H_ϕ fields along three different lines: Figure 8a, $z = 20$–1000 m and $\rho = 0.15$ m fixed; Figure 8b,

$z = 20$–1000 m and $\rho = 1000$ m fixed; Figure 8c, $\rho = 20$–2000 m and $z = 1000$ m fixed. One might observe from these figures that for small ρ, the H_ϕ field is much larger with casing than without casing. However, for large ρ, the H_ϕ field is larger without casing than with casing given that z is small. For the case of both large ρ and z, the H_ϕ fields with and without casing are similar in magnitude.

Casing antenna equivalent length and dipole moment

From Ampere's law, the current flowing along the casing can be determined by

$$I_z = 2\pi\rho H_\phi(\rho) \tag{5}$$

for ρ approaching t from outside the casing ($\rho \to t$ and $\rho > t$).

Figure 9 shows the magnitude and the phase of the casing current as a function of z for different values of the product of frequency and relative magnetic permeability (μ_r). The range of the value of the product varies from 1 to 10^4, which corresponds to a frequency range of 0.01 Hz to 100 Hz given a casing with $\mu_r = 100$.

The current is distributed over the whole length of the casing conductor. The dipole moment of a finite-length antenna is defined as IL, the product of the current I and the antenna length L. In our case of a continuous current distribution, we define the casing dipole moment as

$$M_{\text{dipole}} = \int_{-\infty}^{\infty} I(z)dz \equiv I(z=0)D, \tag{6}$$

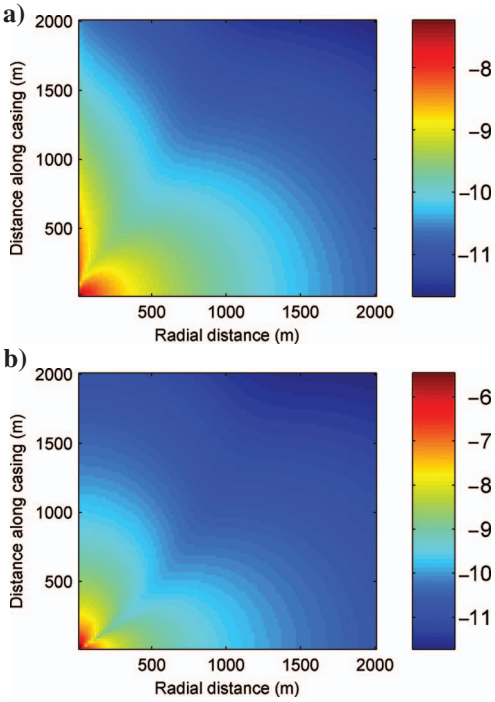

Figure 6. Comparison of the vertical electric field (E_z) distribution for (a) a model with steel casing, with a homogeneous model (b) without steel casing. The VED dipole source is placed inside the casing at the axis origin (radial distance = distance along casing = 0). Color scale is $\log_{10}(|E_z|)$.

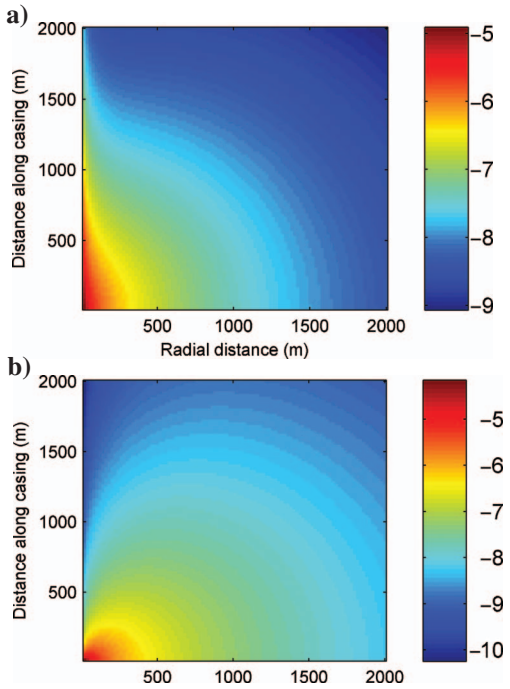

Figure 5. Comparison of the azimuthal magnetic field (H_ϕ) distribution for (a) a model with steel casing, with a homogeneous model (b) without steel casing. The VED source is placed inside the casing at the axis origin (radial distance = distance along casing = 0). Color scale is $\log_{10}(|E_\phi|)$.

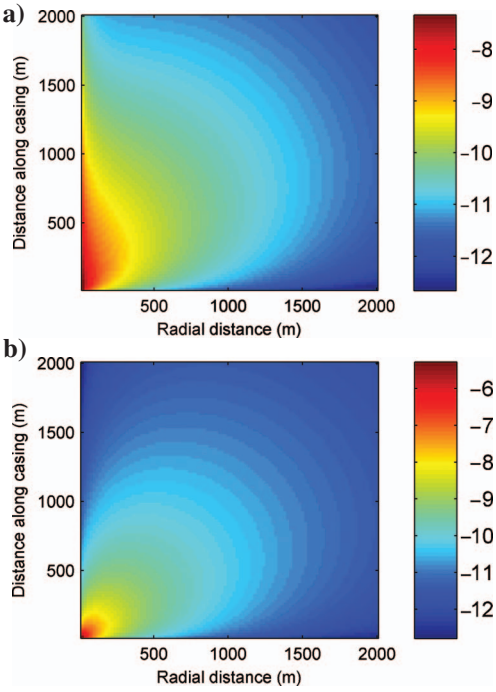

Figure 7. Comparison of the horizontal electric field (E_ρ) distribution for (a) a model with steel casing, with a homogeneous model (b) without steel casing. The VED dipole source is placed inside the casing at the axis origin (radial distance = distance along casing = 0). Color scale is $\log_{10}(|E_\rho|)$.

where the magnitude of D defines what we refer to as the antenna equivalent length. From the definition of the inverse Fourier cosine transform, we obtain

$$\hat{I}(\lambda) = \frac{1}{\pi}\int_{-\infty}^{\infty} I(z)\cos(\lambda z)dz. \quad (7)$$

Setting $\lambda = 0$ leads to $\pi\hat{I}(\lambda = 0) = \int_{-\infty}^{\infty} I(z)dz = M_{\text{dipole}}$. Using Ampere's law, the dipole moment can be written further as

$$M_{\text{dipole}} = 2\pi^2\rho\hat{H}_\phi(\lambda = 0,\rho) \quad \text{for } \rho \to t. \quad (8)$$

Hence, the dipole moment follows directly from the magnetic field in the wavenumber domain, which can be calculated as described in Appendix A.

The current distributions along the casing shown in Figure 9 are approximately exponentially decaying functions, and can be expressed as $I(z) = I_0 e^{-\alpha z}$, where α is the decay index. Given such exponentially decaying current distribution, the dipole moment has the following simple form:

$$M_{\text{dipole}} = \int_{-\infty}^{\infty} I(z)dz = 2\int_{0}^{\infty} I_0 e^{-\alpha z}dz = I_0\frac{2}{\alpha} = I_0 D. \quad (9)$$

The antenna equivalent length is therefore $D = 2/\alpha$.

The decay index α can be calculated numerically. The index values listed in Table 1 were obtained by taking the derivative of the logarithm of the current distribution at $z = 60$ m. It can be seen from Table 1 that the magnitude of the dipole moment is almost unity at the frequency of 0.1 Hz. It decreases to 0.9 A/m at 1 Hz, and reduces quickly for even higher frequencies. At 1000 Hz, the magnitude becomes $1.5(10^{-7})$ A/m. Table 1 also shows the values of the antenna equivalent lengths versus the product of frequency and relative magnetic permeability, obtained from equation 9.

The antenna equivalent length for the DC case also can be calculated using the transmission-line approximation proposed by Kaufman (1990). In that case, the current along the steel casing can be written as

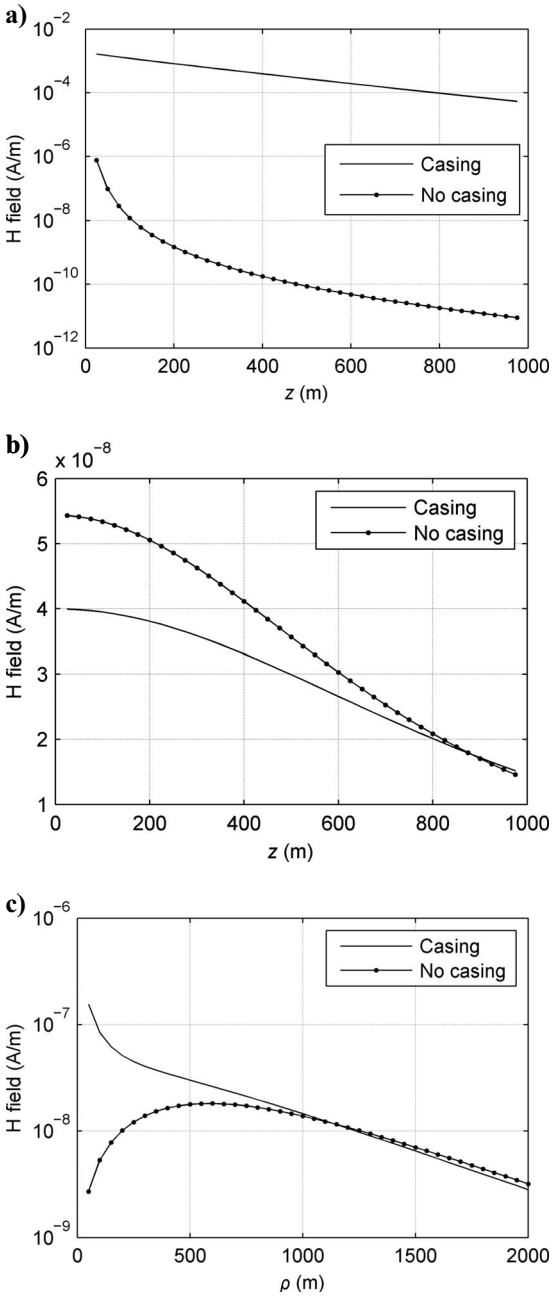

Figure 8. Comparison of the azimuthal magnetic field (H_ϕ) with and without steel casing, at three different lines: (a) H_ϕ versus vertical direction (z) at $\rho = 0.15$ m, (b) H_φ versus vertical direction (z) at $\rho = 1000$ m, and (c) H_ϕ versus horizontal direction (ρ) at $z = 1000$ m.

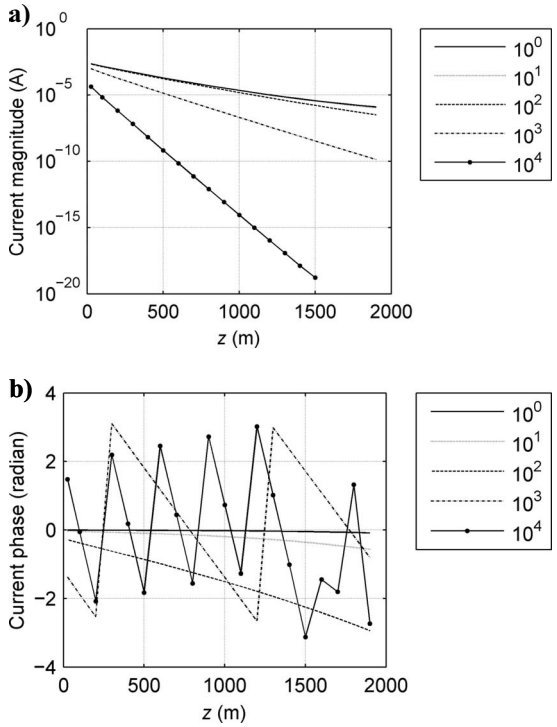

Figure 9. (a) Magnitude and (b) the phase of the current along the casing (generated by a unit-moment VED inside the casing at $z = 0$) for different values of the product of casing magnetic permeability and frequency (μf).

$$I(z) = I_0 \exp\left(-z\sqrt{\frac{\sigma_3}{S_c}}\right), \tag{10}$$

where $S_c = \sigma_2(2\pi s(t-s))$ is the conductivity per unit length of the casing, which has a value of 31416 S/m for our model. According to equation 9, the antenna equivalent length then is

$$D = 2\sqrt{\frac{S_c}{\sigma_3}}, \tag{11}$$

which equates to 354 m for our model parameters, thus confirming our calculation at DC. Referring to Table 1, we note that the antenna equivalent length does not change much for frequencies below 1 Hz. Hence, equation 11 can be used to estimate the antenna equivalent length for low frequencies. Table 1 further shows that the antenna equivalent length is longest for the DC case and decreases for increasing frequencies.

THE CASING EFFECT: TE MODE

The fields generated by a Hertzian magnetic dipole (Wait, 1987) are TE fields, i.e., E_ϕ, H_ρ, and H_z.

The duality principle (Kong, 1990) states that the fields generated by a magnetic dipole can be obtained from the fields generated by an electric dipole as long as the following replacements are made:

$$E \to H, \quad H \to -E, \quad \mu \to \varepsilon, \quad \varepsilon \to \mu. \tag{12}$$

Hence, the TE solution for the casing case can be obtained by using the above-mentioned replacements to the previously derived equations for TM solution. In the quasi-static case,

$$\varepsilon \leftrightarrow \mu \text{ means } \frac{\sigma}{i\omega} \leftrightarrow \mu. \tag{13}$$

Before performing the numerical calculation, we estimate the effect of the above replacement on the final solutions. First, it can be seen that (Appendix A) equation A-11 remains unchanged because the term $i\omega\mu\sigma$ is invariant to the replacement. However, in the (Appendix A) equation A-8, the conductivity now is replaced by the magnetic permeability. We note that the conductivity contrast between the steel casing and the surrounding material can be greater than 10^6, whereas the contrast in magnetic permeability is only about 10^2. Hence, in the TE case, the steel casing introduces a much smaller contrast with the surrounding material than in the TM case.

It can be shown that the E_ϕ field distributions with and without casing are very similar. The amplitude ratio of E_ϕ with casing to E_ϕ without casing is within the range 0.986 to 0.988 in the ρ-z plane ($f = 1$ Hz). Similar phenomena can be observed for the other field components. From Table 2, one can see that for frequencies of 1 Hz and below, the casing has little effect on shielding the magnetic dipole source inside the casing, but it starts to have a noticeable effect (E_ϕ reduction factor of 2) when 10 Hz is used and a very large effect when 100 Hz is used. Given a frequency of 100 Hz, the amplitude ratio of E_ϕ with casing to E_ϕ without casing is about 0.02 at the location $x = 20$ m and $z = 20$ m. For $z > 20$ m and $x > 20$ m, this amplitude ratio almost is unchanged. The casing effects for the TE case can be found in many publications (see, e.g., Augustin et al., 1989; Uchida et al., 1991).

DISCUSSION

Casing antenna effects

From Table 1, we can see that the casing effects on the source radiation are twofold. One is that the casing dipole moment is reduced compared to the dipole moment of the current source. This can be considered as the casing attenuation effect. The other is that the casing changes the field distribution patterns. This is because for the TM mode, the casing acts as a long antenna having an equivalent length as defined by equation 6. The second effect has a negative impact on the detection resolution and is discussed in more detail later.

It is sometimes mentioned that the steel-casing effect of an induction coil is localized, and limited to a small distance (less than 1 m) above and below the induction source (see, for example, Kirkendall et al., 1999). This conclusion is correct only for the TE case. For the TM case, the casing effect is a nonlocal effect. In Table 1, we see that even at a high frequency of 1000 Hz, the antenna equivalent length still has a large value.

We noted before that the antenna equivalent length is not changed much from DC to 1 Hz. However, from Table 1, we see that the phase of the casing current changes noticeably around 1 Hz. This suggests that the frequency of 1 Hz lies in a transition zone from the DC approximation to the HF approximation for the cases considered

Table 1. Equivalent lengths and dipole moments of casing antennas.

Frequency (Hz)	DC	0.01	0.1	1	10	100	1000
Product: $f\mu_r$	0	1	10	100	10^3	10^4	10^5
Decay index: α (m^{-1})	0.0057	0.0057	0.0057	0.0060	0.0118	0.032	0.093
Antenna equivalent length: $2/\alpha$ (m)	352	352	351	333	170	62.9	21.5
Dipole moment (Magnitude: A/m)	0.999	0.994	0.994	0.880	0.210	0.005	1.5 (10^{-7})
Dipole moment (Phase: radians)	0.000	− 0.006	− 0.057	− 0.490	− 1.831	1.306	− 2.052

Table 2. Amplitude ratio and phase difference between casing and noncasing for E_φ field at $x = 20$ m and $z = 20$ m generated by a magnetic dipole at axis origin.

Frequency (Hz)	0.1	1	10	100
Amplitude ratio for $\sigma_2 = 5\times10^6$	1.00	0.99	0.50	0.02
Amplitude ratio for $\sigma_2 = 10^6$	1.00	1.00	0.95	0.26
Phase difference (radians) for $\sigma_2 = 5\times10^6$	− 0.02	− 0.21	− 1.44	1.67
Phase difference (radians) for $\sigma_2 = 10^6$	0.00	− 0.04	− 0.41	− 2.08

here. Appendix B gives further arguments for considering the frequency range 0.1–10 Hz as a transition zone between DC and HF approximations.

In the terminology of antenna engineering, equation 7 shows the relation between the antenna current and the space factor of the radiation pattern (Balanis, 1997). It can be proved that the space factor for the direction normal to the current direction (usually the direction of maximum radiation power) remains invariant when using the dipole-moment expression 6 to represent an infinitely distributed current.

Casing effect on characterizing resistive layers

The casing attenuation effect is moderate for our frequency band. Even at the highest frequency of 10 Hz, the reduction factor of the dipole moment is not more than 5 for the TM mode (see Table 1).

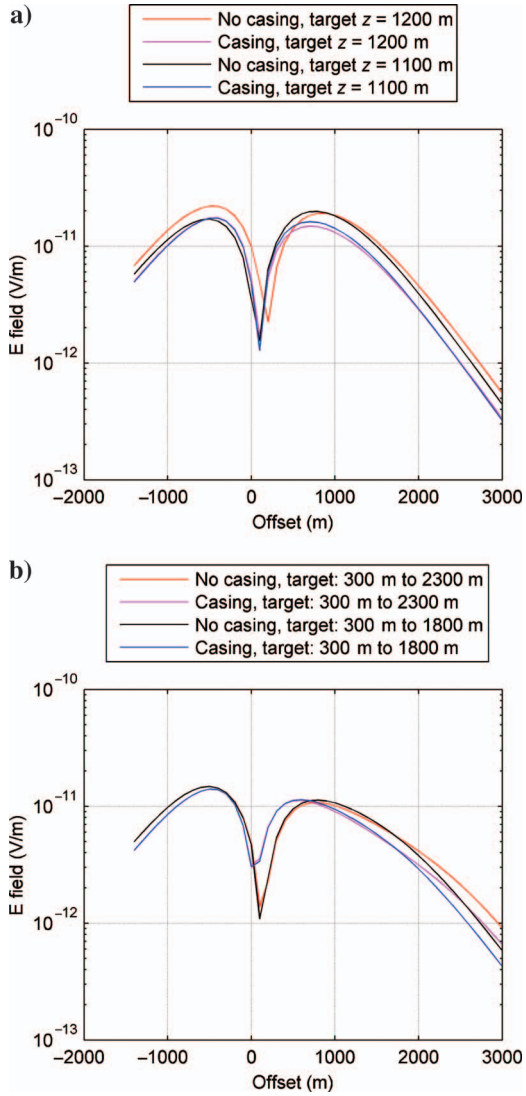

Figure 10. Comparison of the horizontal electric field at seabed versus offset, with and without casing, for four cases: (a) Cases 1 and 2 with target depths at $z = 1200$ m and $z = 1100$ m, respectively. The lateral extension of target is 1000 m. (b) Cases 3 and 4 with lateral extensions of targets 2000 m and 1500 m, respectively. Target depth is $z = 1200$ m. In all simulations, a 1 Hz-VED source placed inside the casing at $z = 1200$ m is used, and target is 100 m thick with resistivity of 100 ohm-m.

Because of the large effective antenna length, the near-field resolution will be degraded. However, for the far-field, the angular resolution is not necessarily reduced. As in conventional antenna engineering, large antennas are used to achieve a better far-field angular resolution. In the situation of measuring EM signals inside a casing for characterization of 2D hydrocarbon layers, we have used a finite-element solver (Kong et al., 2008) developed for 2.5D problems. The casing current, a distributed current along the casing conductor, is used as the source terms for the solver. We should mention that this way of treating the target detection is only approximate because the casing current is calculated by assuming that the formation outside the casing is homogeneous. However, when the inhomogeneous parts of the formation have some distance (one or a few skin depths) from the source inside the casing, then this method can be sufficiently accurate. One might conjecture that the casing current would not change dramatically even when the cased borehole intersects the reservoir because only a small amount of current can flow into the resistive reservoir, compared to the current flowing into the conductive formation.

Figure 10a shows the casing effect on detecting layers at different depths for the following model: a vertical electric dipole source at $z = 1200$ m, water depth 500 m ($z_{\text{seabed}} = 0$ m), and frequency 1 Hz. For case 1, the target is at $z = 1200$ m, and for case 2, the target is at $z = 1100$ m. The E_x field is recorded on the seabed at different offsets. The target is 100 m thick, extends from $x = 100$ m to $x = 1100$ m, and has a resistivity of 100 ohm-m. From the figure, it can be seen that for these two targets at different depths, the fields received on the seabed are not very different. Hence, we could say that the vertical resolution is degraded because of the casing. Without casing, it is possible to resolve the two targets much better in depth.

Figure 10b shows the casing effect on detecting layers with different horizontal extent. Now both targets are at $z = 1200$ m, but for case 1, the target is at $x = 300$–2300 m, and for case 2, the target is at 300–1800 m. From the figure, it can be seen that the horizontal resolution is not changed much by the casing. The target edge at the far offset can be detected clearly for both target cases independent of whether casing is present or not.

Relevance to actual measurements

An actual borehole receiver for the sea-to-borehole method should be capable of measuring both TM and TE mode fields as can be accomplished, e.g., by a pair of electrodes in combination with an induction coil for measuring both the electric field and the magnetic field along the borehole axis. Note that such sensor combination captures TE and TM modes even in deviated or horizontal wells.

The results obtained from this study can be useful for actual sea-to-borehole measurements. First of all, the derived casing current can serve as the source term for existing modeling tools to perform forward modeling for planning actual measurements. This application has been discussed in the previous section. The casing effect as a function of the frequency and the casing magnetic property can be used as a guideline for choosing the measurement frequency. In the case of using receiver arrays, the findings of this study suggest that it is not advantageous to have dense TM mode receivers because the resolution is limited by the steel casing. Instead, one should use long separation between the electrodes within a single receiver unit to increase the dipole moment of the electrode pair.

CONCLUSION

Given a sufficient signal-to-noise ratio, the sea-to-borehole CSEM method has the potential of becoming a useful new exploration and monitoring technique. The method also might be considered in combination with the existing marine CSEM method, i.e., a configuration whereby receivers are deployed both in a borehole and on the seabed. Our modeling shows that the EM fields at reservoir depth can be 1-2 orders of magnitude larger than those on the seabed, thus opening up the possibility to see deeper and to detect and monitor smaller targets. Further analysis of the casing effects demonstrates that in our frequency range of interest (0.1–10 Hz), this increase in field strength is not lost to the casing attenuation for either the TM mode or the TE mode.

We have shown, however, that the field distributions in the TM mode are changed very much with the presence of a steel casing. The reason is that a current is induced which flows along a conductive casing, and decays rather slowly. In the TM mode, the casing problem can be treated in two steps. The first is to find the current induced from an electric dipole source inside the casing. The second is to find the target response from the casing current. In the second step, the casing is considered as an antenna. We then calculate the dipole moment and the equivalent length of the "casing antenna." In the frequency range used, the antenna equivalent length can be as long as a few hundred meters. This will degrade the vertical resolution in detecting the target layer. The ratio of the dipole moment of the casing antenna to that of the excitation antenna can be considered as the casing attenuation effect. The ratio is not far from unity for frequencies smaller than 1 Hz. However, the ratio decreases rapidly with frequency. For example, the ratio is 0.21 at 10 Hz.

When using very low frequencies, the results derived here approach the DC limit (the transmission-line approximation). Criteria are derived to define the frequency range for DC approximation and the frequency range for HF approximation. The used frequency range of 0.1 Hz to 10 Hz lies within the transition range from the DC approximation to the HF approximation.

The TE solution can be obtained from the TM solution by using the duality principle. The numerical results show that for the TE mode, the field distributions are far less affected by the casing than for the TM mode. The ratio of E_φ field magnitude for cases with and without casing is 0.5 at 10 Hz.

We have shown that despite the loss in vertical resolution by the casing, the lateral resolution of TM measurements remains largely unchanged and seems sufficient to outline the edges of a resistive target. The TE mode measurement, having a localized casing effect, contributes valuable information about the background resistivity, and about the target resistivity when using an inclined borehole to characterize an arbitrarily shaped target.

ACKNOWLEDGMENTS

The authors wish to thank the Norwegian Research Council, StatoilHydro, Shell, EMGS, Sensor Development, and NGI for the financial support through a Petromaks project. The authors thank Johan van Popta, Mathieu Darnet, and Joonsang Park for their comments on the manuscript.

APPENDIX A

THEORY TO SOLVE THE CASING PROBLEM IN TM MODE

Consider an electric current source along the z-direction inside an infinitely long and vertical steel casing with the following model parameters:

s = inner radius
t = outer radius
σ_1 = conductivity of the borehole fluid
σ_2 = conductivity of the steel casing
σ_3 = conductivity of the formation
$\mu = \mu_r \mu_0$ = magnetic permeability of the casing, where μ_r is the relative permeability and $\mu_0 = 4\pi 10^{-7}$ H/m is the magnetic permeability in vacuum.

We use the Debye potential U (Wait, 1987), which is the z-component of the Hertz vector resulting from a current source, to derive the TM fields H_ϕ, E_ρ, and E_z in cylindrical coordinates:

$$H_\phi = -\sigma \frac{\partial U}{\partial \rho}, \tag{A-1}$$

$$E_\rho = \frac{\partial^2 U}{\partial \rho \partial z}, \tag{A-2}$$

$$E_z = \left(k^2 + \frac{\partial^2}{\partial z^2}\right) U, \tag{A-3}$$

where

$$k^2 = -i\omega\sigma\mu. \tag{A-4}$$

Because the configuration is invariant along the vertical direction, it is convenient to consider the Fourier cosine transform of the Debye potential:

$$U(z) = \int_0^\infty \hat{U}(\lambda)\cos(\lambda z) d\lambda. \tag{A-5}$$

In later discussions, a function with "hat," such as $\hat{U}(\lambda)$ in equation A-5, and the original function with no "hat," such as $U(z)$, define a Fourier transform pair.

We derive a solution of the form

$$\hat{U}(\lambda) = aK_0(k_\rho \rho) + bI_0(k_\rho \rho), \tag{A-6}$$

where K_0 and I_0 are, respectively, the zero order, second and first modified Bessel functions, and

$$k_\rho = \sqrt{-k^2 + \lambda^2}. \tag{A-7}$$

In equation A-6, the constants "a" and "b" can be used to match the boundary conditions. Equations A-1–A-3 now become

$$\hat{H}_\phi = -\sigma[-ak_\rho K_1(k_\rho \rho) + bk_\rho I_1(k_\rho \rho)], \tag{A-8}$$

$$\hat{E}_\rho = \lambda[ak_\rho K_1(k_\rho \rho) - bk_\rho I_1(k_\rho \rho)], \tag{A-9}$$

and

$$\hat{E}_z = -k_\rho^2[aK_0(k_\rho\rho) + bI_0(k_\rho\rho)]. \quad \text{(A-10)}$$

To derive the above equations, the following relations have been accounted for: $I_0' = I_1$ and $K_0' = -K_1$.

We refer to "a" as the coefficient for the outward wave and "b" as the coefficient for the inward (reflected) wave. There is no reflected wave in the third layer and the constant "b_3" becomes zero. Hence, for this three-layer model, five coefficients need to be calculated: a_1, b_1, a_2, b_2, and a_3. We use equations A-4 and A-7 to define k_ρ in layers 1, 2, and 3 as

$$k_n = \sqrt{i\omega\mu\sigma_n + \lambda^2} \quad \text{for } n = 1,2,3. \quad \text{(A-11)}$$

The coefficient a_1 can be determined by the boundary condition at the source location. When the distance R to the source approaches zero, the Debye potential can be written as (Wait, 1987)

$$U = \frac{IL}{4\pi\sigma R}, \quad \text{(A-12)}$$

where I is the current, L is the dipole length, IL is the dipole moment, and σ is the conductivity surrounding the dipole. We assume the dipole moment of the electric current source is unity.

In the first layer, we have

$$\hat{U} = a_1K_0(k_\rho\rho) + b_1I_0(k_\rho\rho). \quad \text{(A-13)}$$

When ρ approaches zero, the term $a_1K_0(k_\rho\rho)$ dominates. Using equation A-13 and the following equation (Wait, 1982),

$$\frac{1}{R} = \frac{1}{\sqrt{\rho^2 + z^2}} = \frac{2}{\pi}\int_0^\infty K_0(\lambda\rho)\cos(\lambda z)d\lambda, \quad \text{(A-14)}$$

in equation A-12, we derive

$$a_1 = \frac{IL}{2\pi^2\sigma_1}. \quad \text{(A-15)}$$

Now that a_1 is determined, the four other coefficients can be determined by the boundary conditions at the casing walls, i.e., both E_z and H_ϕ are continuous at the inner wall ($\rho = s$), and at the outer wall ($\rho = t$). After all the coefficients are obtained, we then have the potential U in the third layer:

$$\hat{U} = a_3K_0(k_3\rho). \quad \text{(A-16)}$$

From equations A-8–A-10, the fields outside the casing thus are given by

$$\hat{H}_\phi = -\sigma\frac{\partial\hat{U}}{\partial\rho} = a_3\sigma_3k_3K_1(k_3\rho), \quad \text{(A-17)}$$

$$\hat{E}_\rho = \frac{\partial^2\hat{U}}{\partial\rho\partial z} = a_3\lambda k_3K_1(k_3\rho), \quad \text{(A-18)}$$

and

$$\hat{E}_z = \left(k^2 + \frac{\partial^2}{\partial z^2}\right)\hat{U} = -a_3k_\rho^2K_0(k_3\rho). \quad \text{(A-19)}$$

APPENDIX B

DC AND HF APPROXIMATION

To find the valid frequency ranges for the DC approximation and for the HF approximation, we use the results concerning the internal impedance of a round wire (Ramo et al., 1994). The impedance of a round wire can be calculated using the analytic method described previously. For a simplified case assuming no field variation along z (i.e., $k_z = 0$), we can write

$$Z_i \approx \frac{1}{S_c}\left[1 + \frac{1}{48}\left(\frac{t-s}{\delta}\right)\right] + j\frac{\omega\mu_r\mu_0}{8\pi}, \quad \text{(B-1)}$$

where δ is the skin depth of the casing steel and S_c is the casing conductance per-unit length defined for equation 10 in the main text.

The first term is the DC resistance per-unit length, and the second is a correction term useful only for the case when the casing thickness is in the order of the skin depth δ. For our case, this term can be omitted. The third is the internal inductance. When setting the imaginary part equal to the real part, a characteristic transition frequency can be determined as

$$f_c = \frac{4}{S_c\mu_0\mu_r}. \quad \text{(B-2)}$$

The calculated frequency is 1.01 Hz for our model (casing conductivity $5(10^6)$ S/m and relative permeability $\mu_r = 100$). Hence, using 0.1 Hz will lead to the real part of equation B-1 being 10 times larger than the imaginary part, and we use this as the criterion to define the highest frequency for the DC approximation. When using 10 Hz, then the real part of equation B-1 will be 1/10 of the imaginary part, and we use this as the criterion to define the lowest frequency for the HF approximation. Hence, our frequency range (0.1–10 Hz) actually is within a transition frequency band from the DC approximation to the HF approximation.

REFERENCES

Alumbaugh, D. L., and H. F. Morrison, 1995, Crosswell electromagnetic tomography: Theoretical and practical considerations for cylindrical geometry: Geophysics, **60**, 846–870.

Augustin, A. M., W. D. Kennedy, H. F. Morrison, and K. H. Lee, 1989, A theoretical study of surface-to-borehole electromagnetic logging in cased holes: Geophysics, **54**, 90–99.

Balanis, C. A., 1997, Antenna theory: John Wiley & Sons, Inc.

Becker, A., B. Wang, K. H. Lee, and M. Wilt, 1997, Subsurface electromagnetic measurement through steel casing: 67th Annual International Meeting, Expanded Abstracts, 1965–1968.

Chave, A. D., and C. S. Cox, 1982, Controlled electromagnetic sources for measuring electrical conductivity beneath the oceans: Part 1—Forward problem and model study: Journal of Geophysical Research, **87**, no. B7, 5327–5338.

Chew, W. C., 1995, Waves and fields in inhomogeneous media: IEEE Press.

Constable, S., and L. J. Srnka, 2007, An introduction to marine controlled-source electromagnetic methods for hydrocarbon exploration: Geophysics, **72**, no. 2, WA3–WA12.

Eidesmo, T., S. Ellingsrud, L. M. MacGregor, S. Constable, M. C. Sinha, S. Johanson, F. N. Kong, and H. Westerdahl, 2002, Sea Bed Logging (SBL), a new method for remote and direct identification of hydrocarbon filled layers in deepwater areas: First Break, **20**, 144–152.

Ellingsrud, S., T. Eidsmo, S. Johansen, M. C. Sinha, L. M. MacGregor, and S. Constable, 2002, Remote sensing of hydrocarbon layers by seabed logging (SBL): Results from a cruise offshore Angola: The Leading Edge, **21**, 972–982.

Hoversten, G. M., G. A. Newman, H. F. Morrison, E. Gasperikova, and J. I. Berg, 2001, Reservoir characterization using crosswell electromagnetic inversion: A feasibility study for the Snorre field, North Sea: Geophysics, **66**, 1177–1189.

Kaufman, A. A., 1990, The electrical field in a borehole with a casing: Geophysics, **55**, 29–38.
Kaufman, A. A., and W. E. Wightman, 1993, A transmission-line model for electrical logging through casing: Geophysics, **56**, 1739–1747.
Kirkendall, B., P. Harben, and P. Lewis, 1999, Advances in crosswell electromagnetics: Steel cased boreholes: 69th Annual International Meeting, SEG, Expanded Abstracts, 323–326.
Kong, F. N., 2007, Hankel transform filters for dipole antenna radiation in a conductive medium: Geophysical Prospecting, **55**, 83–89.
Kong, F. N., S. E. Johnstad, and T. Røsten, 2007, Characteristics of scattered fields from hydrocarbon layers in seabed logging: PIERS Online, 2, 585–588 accessed 15 June 2009; http://piers.mit.edu/piersonline/piers.php?volum=2&number=67page=585, doi: 10.2529/PIERS060821070831.
Kong, F. N., S. E. Johnstad, T. Røsten, and H. Westerdahl, 2008, A 2.5D finite-element-modeling difference method for marine CSEM modeling in stratified anisotropy media: Geophysics, **73**, no. 1, F9–F19.
Kong, F. N., H. Westerdahl, S. Ellingsrud, T. Eidesmo, and J. Johansen, 2002, Seabed logging: A possible direct hydrocarbon indicator for deepsea prospects using EM energy: Oil and Gas Journal, **100**, 30–38.
Kong, J. A., 1972, Electromagnetic fields due to dipole antennas over stratified anisotropic media: Geophysics, **37**, 985–996.
——–, 1990, Electromagnetic wave theory: 2nd ed.: John Wiley & Sons, Inc.
Lee, K. H., H. J. Kim, and T. Uchida, 2005, Electromagnetic fields in a steel-cased borehole: Geophysical Prospecting, **53**, 13–21.
Lien, M., and T. Mannseth, 2008, Sensitivity study of marine CSEM data for reservoir production monitoring: Geophysics, **73**, no. 4, F151–F163.
Løseth, L. O., and L. Amundsen, 2007, On the signal propagation in marine CSEM: 69th Conference and Exhibition, EAGE, Extended Abstracts, D035.
MacGregor, L., and S. Sinha, 2000, Use of marine controlled-source electromagnetic sounding for sub-basalt exploration: Geophysical Prospecting, **48**, 1091–1106.
Newman, G. A., 1995, Crosswell electromagnetic inversion using integral and differential equations: Geophysics, **60**, 899–911.
Orange, A., K. Key, and S. Constable, 2009, The feasibility of reservoir monitoring using time-lapse marine CSEM: Geophysics, **74**, no. 2, F21–F29.
Pardo, D., C. Torres-Verdín, and L. Demkowicz, 2007, Feasibility study for two-dimensional frequency-dependent electromagnetic sensing through casing: Geophysics, **72**, no. 3, F111–F118.
Pardo, D., C. Torres-Verdín, and Z. Zhang, 2008, Sensitivity study of borehole-to-surface and crosswell electromagnetic measurements acquired with energized steel casing to water displacement in hydrocarbon-bearing layers: Geophysics, **73**, no. 6, F261–F268.
Ramo, S., J. R. Whinnery, and T. V. Duzer, 1994, Fields and waves in communication electronics, 3rd ed.: John Wiley & Sons, Inc.
Schenkel, C. J., and H. F. Morrison, 1994, Electrical resistivity measurement through metal casing: Geophysics, **59**, 1072–1082.
Scholl, C., and R. N. Edwards, 2007, Marine downhole to seafloor dipole-dipole electromagnetic methods and the resolution of resistive targets: Geophysics, **72**, no. 2, WA39–WA49.
Singer, B. S., and K.-M. Strack, 1998, New aspects of through-casing resistivity theory: Geophysics, **63**, 52–63.
Spies, B. R., and T. M. Habashy, 1995, Sensitivity analysis of cross-well electromagnetics: Geophysics, **60**, 834–845.
Stalheim, S. O., and P. A. Olsen, 2008, Sea to borehole application of marine controlled source EM method: 3rd Saint Petersburg Conference & Exhibition, EAGE, Extended Abstracts, C009.
Stratton, J. A., 1941, Electromagnetic theory: McGraw-Hill.
Uchida, T., K. H. Lee, and M. J. Wilt, 1991, Effect of a steel casing on crosshole EM measurement: 61st Annual International Meeting, SEG, Expanded Abstracts, 442–445.
Wait, J. R., 1966, Fields of a dipole over an homogeneous anisotropic half-space: Canadian Journal of Physics, **44**, 2387–2401.
——–, 1982, Geo-electromagnetism: Academic Press.
——–, 1987, Electromagnetic wave theory: John Wiley and Sons, Inc.
Wilt, M. J., D. L. Alumbaugh, H. F. Morrison, A. Becker, K. H. Lee, and M. Deszcz-Pan, 1995, Crosshole electromagnetic tomography: System design considerations and field results: Geophysics, **60**, 871–885.
Wu, X., and T. M. Habashy, 1994, Influence of steel casings on electromagnetic signals: Geophysics, **59**, 378–390.
Zhou, Q., 1989, Audio frequency numerical modeling and tomographic inversion for reservoir evaluation: Ph.D. thesis, University of California, Berkeley.